

# The “angular size - redshift” relation for compact radio structures in quasars and radio galaxies <sup>★</sup>

L. I. Gurvits<sup>1,2</sup>, K. I. Kellermann<sup>3</sup>, and S. Frey<sup>4,1</sup>

<sup>1</sup> Joint Institute for VLBI in Europe, P.O. Box 2, 7991 PD Dwingeloo, The Netherlands

<sup>2</sup> Astro Space Center, P.N. Lebedev Physical Institute, Moscow 117924, Russia

<sup>3</sup> National Radio Astronomy Observatory, 520 Edgemont Road, Charlottesville, Virginia 22903-2475, USA

<sup>4</sup> FÖMI Satellite Geodetic Observatory, P.O. Box 546, H-1373 Budapest, Hungary

Received 24 Jun 1998 / Accepted 05 Oct 1998

**Abstract.** We discuss the “angular size - redshift” relation for compact radio sources distributed over a wide range of redshifts  $0.011 \leq z \leq 4.72$ . Our study is based on a sample of 330 5 GHz VLBI contour maps taken from the literature. Unlike extended source samples, the “angular size - redshift” relation for compact radio sources appears consistent with the predictions of standard Friedmann world models with  $q_0 \simeq 0.5$  without the need to consider evolutionary or selection effects due to a “linear size - luminosity” dependence. By confining our analysis to sources having a spectral index,  $-0.38 \leq \alpha \leq 0.18$ , and a total radio luminosity,  $Lh^2 \geq 10^{26}$  W/Hz ( $H_0 = 100 h \text{ km s}^{-1} \text{ Mpc}^{-1}$ ,  $q_0 = 0.5$  used as a numerical example), we are able to restrict the dispersion in the “angular size - redshift” relation. The best fitting regression analysis in the framework of the Friedmann-Robertson-Walker model gives the value of the deceleration parameter  $q_0 = 0.21 \pm 0.30$  if there are no evolutionary or selection effects due to a “linear size - luminosity”, “linear size - redshift” or “linear size - spectral index” dependence.

**Key words:** quasars: general - galaxies: active - radio continuum: galaxies - cosmology

## 1. Introduction

Classical tests of cosmological world models using the observed dependence of the angular size of galaxies or kiloparsec-scale radio sources have been inconclusive. At optical wavelengths, observational uncertainties at large redshift are large due to the small size of a galactic disk, seeing, the difficulty in defining a true metric rod, and possible evolutionary effects (e.g. Sandage 1988). At radio wavelengths, the separation of the lobes of extended

double radio sources may be determined with great accuracy even at large redshift, but the interpretation of the “angular size - redshift” ( $\theta - z$ ) relation for double radio sources has been obscured by possible selection and evolutionary effects. The observed  $\theta - z$  relation for double radio sources appears to follow a simple  $1/z$  law even at high redshift, in apparent contradiction to any simple Friedmann-Robertson-Walker (FRW) model without evolution (e.g. Kapahi 1989). Most researchers interpret the observed  $\theta - z$  diagram for double radio sources as evidence for a decrease in linear size with redshift (Kapahi 1987, Barthel and Miley 1988, Neeser et al. 1995). However, Singal (1993) and Nilsson et al. (1993) consider that the observed departure from the FRW curves is due to an inverse “linear size - luminosity” correlation which preferentially selects the smaller (high luminosity) sources at high redshifts. It is curious, however, that these selection or evolutionary effects apparently combine with cosmological effects to give the simple observed  $1/z$  relation.

More recently, Buchalter et al. (1998) have studied a sample of 103 double lobed quasars with  $z > 0.3$  using the VLA at 20 cm in its B-configuration. In contrast to the  $1/z$  “angular size - redshift” relation found for double lobed radio sources by other workers, Buchalter et al. find no change in apparent angular size in the range of  $1.0 \lesssim z \lesssim 2.7$ , consistent with FRW models without significant evolution. But, it is not clear to what extent their results are affected by the limited range of angular size, between 12 and 120 arcseconds, which can be observed with the VLA in the B-configuration at 20 cm.

The size of extended double lobe source whose linear extent is typically hundreds of kiloparsecs, may depend on the systematic changes in the properties of the intergalactic medium with  $z$ . Moreover, high redshift extended sources have ages which are comparable to the age of the Universe, and so evolutionary effects are not unexpected. Compact radio jets associated with quasars and AGN, by contrast, are typically less than a hundred parsec in extent. Their morphology and kinematics probably depends more on the nature of the “central engine” than on the sur-

*Send offprint requests to:* L. I. Gurvits, 1st address, lgurvits@jive.nfra.nl

<sup>★</sup> Table 1 is available in electronic form at the CDS via anonymous ftp to [cdsarc.u-strasbg.fr](http://cdsarc.u-strasbg.fr) (130.79.128.5) or via <http://cdsweb.u-strasbg.fr/Abstract.html>

rounding intergalactic medium. The “central engine” itself is thought to be controlled by a limited number of physical parameters, such as the mass of central black hole, the strength of magnetic field, the accretion rate, and, possibly, the angular momentum. This central region may be “standard” for sources in which these parameters are confined within restricted ranges. Also, because the compact radio jets have typical ages of only some tens of years, they are young compared to the age of the Universe, at any reasonable redshift. Therefore, compact radio sources may offer an evolution free sample to test world models over a wide range of redshift.

However, the size of compact radio jets is not unambiguously defined and depends on the frequency of observation as well as on resolution. Moreover, differences in the spectral index between the core and jet components may introduce a K-like correction which can be important for high redshift sources, as this may introduce an apparent “linear size – redshift” dependence even in the absence of evolution (Kellermann 1993). Frey et al. (1997) have shown that this is likely to be a weak dependence, however more detailed images at various frequencies with matched resolution be needed to verify the importance of any K-like correction.

In several previous studies we have reported on the observed  $\theta - z$  relation for compact radio sources. Kellermann (1993) studied a sample of 79 quasars and AGN’s which had been observed with VLBI at 5 GHz and which have a 5 GHz luminosity greater than  $10^{24}$  W/Hz. There are only a few sources at low redshift which meet the luminosity restriction, but these are consistent with a  $1/z$  relation, characteristic of the Euclidean geometry which describes the local Universe. The Kellermann (1993) sample already includes all sources with luminosity greater than  $10^{24}$  W/Hz at redshifts less than a few tenths, and further surveys down to fainter flux density limits will not find any additional sources which satisfy the luminosity criteria. The important point of the Kellermann (1993) paper was that for redshifts in the range  $0.5 < z < 3$ , the angular size appears to be essentially independent of redshift, in contrast to the  $\theta - z$  relation for powerful extended sources which continues its apparent Euclidean form out to large redshifts. Kellermann noted that the observed form of the  $\theta - z$  relation for the compact source sample was qualitatively consistent with a standard FRW cosmology with  $\Omega = 1$  without the need to appeal to arguments based on size evolution or a “linear size – luminosity” dependence. A more rigorous quantitative analysis of this data by Stepanas and Saha (1995) find a best fit of  $q_0 = 2.6_{-2.2}^{+2.1}$  with the 90% confidence, and they exclude the simple  $\theta \propto 1/z$  relation at the 99% confidence level. Using the same data, Kayser (1995) has applied a Kolmogorov-Smirnov test to compare the linear sizes of high ( $z > 0.75$ ) and low ( $z < 0.75$ ) redshift compact radio sources for different cosmological models and also con-

cludes that the available data allow models with a wide range of  $\Omega$  and the cosmological constant,  $\Lambda$ .

In a separate investigation, Gurvits (1993) used two point VLBI visibility data obtained at 13 cm (Preston et al. 1985) for 337 sources in order to show qualitatively that the observed data suggests  $q_0 \leq 0.5$ . A four-parameter regression analysis of the same sample gave a value of  $q_0 = 0.16 \pm 0.71$  (Gurvits 1994). The same analysis also gave estimates of the dependence of the apparent angular sizes of compact sources on their luminosity and emitting frequency.

More recently, Wilkinson et al. (1998) have reported on the  $\theta - z$  relation for sources taken from the Caltech-Jodrell Bank VLBI CJF sample of 160 flat spectrum radio sources (Taylor et al. 1996 and references therein). As in the studies of Kellermann (1993) and Gurvits (1994), Wilkinson et al. find no dependence of angular size on redshift for sources with  $0.5 < z < 3$ , but conclude that uncertainties in defining the angular size of complex jets, in the K-like correction, in a possible “size – luminosity” dependence, in the effects of orientation, as well as in possible size or luminosity evolution restrict the usefulness of compact sources to accurately constrain the value of  $q_0$ . Dabrowski, Lasenby, and Saunders (1995), as well, have pointed out the difficulty in obtaining a meaningful constraint on  $\Omega$  due to the effects of relativistic beaming in limited source samples.

Krauss and Schramm (1993) and Stelmach (1994) have pointed out that if evolutionary effects can be ruled out, then the form of the “angular size – redshift” relation can put significant limits on the value of the cosmological constant,  $\Lambda$ , as well as on  $\Omega$ . Jackson and Dodgson (1996) have shown that while the data presented by Kellermann (1993) are consistent with  $\Omega_0 \sim 1$  and  $\Lambda_0 = 0$ , since there is not a well defined minimum in the  $\theta - z$  dependence, equally good fits to the data are obtained with smaller values of matter density described by  $\Omega_0 < 1$ , and negative values of  $-6 \lesssim \Lambda_0 \lesssim -2$ .

With the aim of better restricting the allowable range of cosmological parameters, we have compiled a new larger sample of sources than used by Kellermann (1993) or by Wilkinson et al. (1998) but with more complete structural data than used by Gurvits (1993, 1994). We note, that the sample discussed here is inhomogeneous as it is based on VLBI images published by various authors using a variety of antenna configurations and different techniques for image reconstruction. In Section 2 we discuss the definition of our sample, and in the following sections we discuss the apparent “angular size – redshift” dependence.

## 2. The source sample

The new list contains all sources found in the literature which were imaged with VLBI at 5 GHz with a nominal resolution of about 1.5 mas in the east-west direction and with a dynamic range of at least 100. The list includes the

all-sky set of 79 sources discussed by Kellermann (1993), but enhanced by more recently published work, mostly by the Caltech–Jodrell Bank group (Xu et al. 1995, Henstock et al. 1995, Taylor et al. 1994, 1996) of sources at declination greater than 35 degrees. We also included in the sample a number of sources published by other authors and our own recent observations of quasars with measured redshifts greater than 3 (Frey et al. 1997, Paragi et al. 1998).

Our sample differs from the compilation of Wilkinson et al. (1998) primarily in that it includes a number of relatively strong sources at declinations south of +35 degrees, and other sources not presented in the CJF sample. By including sources outside the range of CJF declinations we are able to better sample the sparsely populated low redshift (Euclidean) part of the  $\theta - z$  diagram not included in the CJF sample. The observations of Gurvits et al. (1992, 1994), Frey et al. (1997) and Paragi et al. (1998) were made in an attempt to better sample the high redshift part of the  $\theta - z$  diagram which is particularly sensitive to the value of  $q_0$ . In particular, the unambiguous detection of an increase in angular size at the highest redshifts would indicate a value of  $q_0 > 0$ . The increase in the size of our present sample comes at the expense of homogeneity and the need to use published VLBI contour maps instead of the primary data. We have attempted to minimize the effect of these inhomogeneities by using the following criteria.

As in Kellermann (1993), we define the characteristic angular size of each source as the distance between the strongest component, which we refer to as the core, and the most distant component which has a peak brightness greater than or equal to 2% of the peak brightness of the core. For sources which are slightly resolved or unresolved, we adopted the following procedure. We assume that sources are one dimensional. For sources which appear resolved in at least one direction, we estimated the distance of a secondary component from the core, or its upper limit, from the published contours. If the source was not resolved, we took the size of the major axis of the synthesized beam (FWHM) as an upper limit to the size, unless there was additional information which indicated that the source structure axis lies along a specific direction different from the direction of major axis. The latter applies to those sources which show extensions in a particular direction, including an extension along the minor axis of the synthesized beam. In this case we estimated the upper limit of the size as the size of the beam along the direction of extension. Thus, our approach to measuring source size allows for four different cases:

**Case C:** the distance between the core and a 2%-component;

**Case J:** an upper limit of the size measured as the size of the synthesized beam along the direction of apparent extension, most likely – a jet;

**Case L:** an upper limit of the size measured along the major axis of the synthesized beam;

**Case S:** an upper limit of the size measured along the minor axis of the synthesized beam.

For those sources where multi epoch VLBI images are available, we have used the most recent epoch that meets our criteria of sensitivity and dynamic range. Finally, we excluded from our analysis all unresolved sources if the major axis of the primary beam exceeded 2.2 mas (i.e. all cases L with too large a synthesized beam) and sources which are known to be gravitationally lensed.

The resulting sample of 330 sources is presented in Table 1<sup>1</sup>, where we show the IAU source designation and alternative name in columns 1 and 2. The redshift and optical counterpart are given in columns 3 and 4. Columns 5, 6 and 7 give the flux density at 6 and 20 cm (or a footnote for alternative wavelength) and the two-point spectral index,  $\alpha$  ( $S \propto \nu^\alpha$ ), respectively. Columns 8 and 9 give the angular size (or its upper limit) and the one-letter structure code as explained above. In columns 10–13, we list references for redshift, flux densities at 6 and 20 cm, and for the VLBI image respectively.

### 3. Properties of the sample

The distribution of redshifts for the sources in our sample is shown in Fig. 1. The 79 sources used in the analysis of Kellermann (1993) are shown shaded.

The histogram of the spectral index distribution is shown in Fig. 2. We note, that we have used the value of spectral index as calculated, in most cases, from measurements of total flux density on arcsecond or larger angular scales although our discussion of angular dimensions is based on milliarcsecond-scale structures, which account for only part of the total flux. For most of the sources, this distinction is not important as nearly all of the flux density in sources of interest is contained in the compact component. Where relevant, such as for Cyg A, we specifically used the flux density of the core component. In a few special cases marked in column 6, when flux density at 20 cm was not available, the spectral index was calculated between 6 cm and another longer wavelength as explained in the footnotes.

Fig. 3 shows the luminosity of all the sources in our sample as a function of their redshift. (Throughout this paper we use  $H_0 = 100 h \text{ km s}^{-1} \text{ Mpc}^{-1}$  and a deceleration parameter  $q_0 = 0.5$  to calculate the luminosity). The shape of the luminosity – redshift diagram and the narrow dispersion simply reflects the fact that our sample, although compiled on an ad-hoc basis from the literature and based upon various selection criteria, is basically a flux-limited sample.

<sup>1</sup> Table 1 is available in electronic form at the CDS via anonymous ftp to [cdsarc.u-strasbg.fr](http://cdsarc.u-strasbg.fr) (130.79.128.5) or via <http://cdsweb.u-strasbg.fr/Abstract.html>

#### 4. Properties of angular size

In Fig. 4, we plot the measured angular size against redshift for all 330 sources in our sample. For the well resolved sources, the procedure of measuring  $\theta$  gives an unambiguous estimate of a metric size. But, for sources with maximum dimensions comparable to or smaller than the beam size, there are large uncertainties. For this reason, and to minimize the influence on our analysis of the few sources with extremely large dimensions, we have chosen to bin the data and to examine the change in median angular size with redshift. This allows us to treat equally true metric sizes of resolved sources and upper limits of sizes for slightly resolved or unresolved ones. Fig. 5 shows the binned data of median angular size plotted against redshift for the same data. (Here and throughout this paper we use nearly equally populated bins, which number is close to  $\sqrt{N}$ , where  $N$  is the size of the sample.) As found in previous studies, for  $z \geq 0.5$ , the median angular size is nearly independent of redshift. In this figure, as an example we show a family of curves for a standard rod in various world models. We note, that none of these curves represent the best fit discussed below.

##### 4.1. “Angular size – luminosity” and “angular size – spectral index” relations

As it is clear from Fig. 3, our sample contains sources with luminosity ranging over more than 4 orders of magnitude. Fig. 6 shows the relation between median angular size and luminosity (the same binning in redshift space as in Fig. 5).

Fig. 7 shows the dependence of the angular size on spectral index. As expected from simple consideration of self absorption arguments, sources with flat and inverted spectra should, on average, have smaller sizes. Fig. 7 qualitatively confirms this expectation. It may also indicate a presence of one or several selection effects. However, as illustrated by Fig. 8, we do not find an evidence on systematic correlation between  $\alpha$  and  $z$ , which might be responsible for the appearance of the “ $\theta - \alpha$ ” dependence, shown in Fig. 7. The only possible exception could correspond to the lowest redshift bin. However, this bin represents sources of considerably lower luminosity (cf. Fig. 3), which could differ intrinsically from their higher redshift counterparts.

##### 4.2. Toward estimating cosmological parameters from the $\theta - z$ relation

The  $\theta - z$  relation based on the data described here is qualitatively consistent with  $0 \leq q_o \leq 1$  and  $\Lambda = 0$  without the need to introduce evolutionary effects. The new data, in agreement with presented earlier by Kellermann (1993), Gurvits (1994) and Wilkinson et al. (1998), do not show clear evidence for an angular size minimum near  $z = 1.25$

as expected for models with  $\Omega = 1$  and  $\Lambda = 0$ . The near asymptotic slope of the  $\theta - z$  relation is more characteristic of models with  $\Omega < 1$  and allows values of  $\Lambda \neq 0$ .

These results are, however, based on very inhomogeneous data obtained by many different observers using different instruments and imaging techniques. New VLBI observations now in progress will improve the accuracy of the observed  $\theta - z$  relation as it will provide a uniform data set for analysis using the  $uv$ -data and images rather than published contour maps.

With all the reservations discussed above, as an example of a cosmological test with the  $\theta - z$  relation on milliarcsecond scale, we consider a multi-parameter regression analysis as described by Gurvits (1994) with modifications made by Frey (1998). It is based on the following phenomenological expression

$$\theta \equiv l_m D^{-1}(z) \propto lh L^\beta (1+z)^n D^{-1}(z) \quad , \quad (1)$$

where  $l_m$  is the metric linear size,  $D$  is the angular size distance,  $lh$  is the linear size scaling factor,  $L$  is the source luminosity. Parameters  $\beta$  and  $n$  represent the dependence of the linear size on the source luminosity and redshift, respectively. For a homogeneous, isotropic Universe ( $q_o > 0$ ) with the cosmological constant,  $\Lambda = 0$ ,  $D(z)$  is given by the usual expression

$$D(z) = \frac{q_o z + (q_o - 1) (\sqrt{1 + 2q_o z} - 1)}{q_o^2 (1 + z)^2} \quad . \quad (2)$$

The regression model (Gurvits 1994, Frey 1998) allows us to fit the  $\theta - z$  relation with four free parameters, the linear size scaling factor  $lh$ , the deceleration parameter  $q_o$  and two parameters related to the physics of compact radio emitting regions,  $\beta$  and  $n$ . The value of  $n$ , in turn, could in principle represent three different physical dependences: (i) a cosmological evolution of the linear size; (ii) a dependence of the linear size on the emitted frequency; and (iii) an impact of sources broadening due to scattering in the propagation medium. The latter effect is not important for our sample with the lowest emitted frequency of 5 GHz (which corresponds to  $z = 0$ ). The distinction between the former two effects is beyond the scope of this paper and will require multifrequency  $\theta - z$  tests.

To minimize any possible dependence of linear size on luminosity, we restrict the regression analysis to sources with  $Lh^2 \geq 10^{26}$  W/Hz. Furthermore, as is evident from Fig. 7, there is an obvious dependence of angular size on spectral index. In order to minimize this effect on the regression, we choose only those sources which form a flat segment of the  $\theta - \alpha$  diagram  $-0.38 \leq \alpha \leq 0.18$  (Fig. 7). This selection criterion also partially excludes from the analysis the lowest redshift bin which represents the highest deviation on the  $\alpha - z$  diagram (Fig. 8). By restricting the range of spectral indices, we are able to further restrict the dispersion in intrinsic size in our analysis. Specifically, we exclude many of the relatively large compact steep

spectrum sources and most compact inverted spectrum sources. There are 145 sources which meet these criteria, their distribution in redshift space is shown in Fig. 9, and the median angular sizes versus redshift is shown in Fig. 10.

As an example, we apply the four parameter regression model for median values of this sub-sample grouped into 12 redshift bins. The best fit values and corresponding  $1\sigma$  errors are:  $lh = 23.8 \pm 17.0$  pc,  $\beta = 0.37 \pm 0.27$ ,  $n = -0.58 \pm 1.0$ , and  $q_0 = 0.33 \pm 0.11$ . This result is in qualitative agreement with similar estimates obtained for an independent sample of sources and different technique of measuring their angular sizes (Gurvits 1994).

In Table 2, we show the results of regression modeling of the same binned sub-sample for the two parameters,  $lh$  and  $q_0$ , for different fixed values of  $\beta$  and  $n$ . The ranges for  $\beta$  and  $n$  shown do not require a substantial evolution of linear sizes with redshift and luminosity. We note, that the range of parameter  $\beta$  used covers the estimate obtained for kiloparsec-scale structures in FR II sources by Buchalter et al. (1998;  $\beta \approx -0.13 \pm 0.06$ ) and is close to the estimate obtained earlier for kiloparsec-scale structures in quasars by Singal (1993;  $\beta \approx -0.23 \pm 0.12$ ). Similarly, our range of the parameter  $n$  is close to the estimates obtained in both papers for kiloparsec-scale structures (Singal 1993, Buchalter et al. 1998). However, one must keep in mind that closeness of these values for kiloparsec-scale structures in double radio sources and in our parsec-scale structures could be superficial since the radio emission on these scales, differed by several orders of magnitude, is governed by different physical processes.

As a test of our method of using median values for binned data, we repeated the same procedure for the sub-sample of 145 sources in which the upper limits of angular size (shown in Table 1 with the sign “<” in column 8) are replaced with an arbitrary value of 0.1 mas. The difference between estimates of  $lh$  and  $q_0$  for this test case and values presented in Table 2 does not exceed 4.1% within the range of  $\beta$  and  $n$  shown in Table 2. We therefore conclude that the use of median values is justified.

Values of  $q_0$  shown in Table 2 should be treated with caution due to the deficiencies of the sample and the method described above. For the simple case with no dependence of the source linear size on the source luminosity and redshift (“true” standard rod,  $\beta = 0$  and  $n = 0$ )  $q_0 = 0.21 \pm 0.30$ . This result does not contradict to the estimate of  $q_0$  in  $\Lambda = 0$ , “no-evolution” ( $\beta = n = 0$ ) by Buchalter et al. (1998). Solutions, which allow evolution of source size with redshift ( $n \neq 0$ ) or a dependence on luminosity ( $\beta \neq 0$ ), favor values of  $q_0 \lesssim 0.5$  for  $\beta + n \gtrsim -0.15$ .

## 5. Summary

The 5 GHz VLBI data are consistent with standard FRW cosmologies with  $0 \lesssim q_0 \lesssim 0.5$  and  $\Lambda = 0$  without the need to introduce evolution of the population or to appeal to

selection effects caused by a possible “luminosity – linear size” dependence. This conclusion is based on the “angular size – redshift” test using an inhomogeneous sample of 330 VLBI images, with the 1.5 mas nominal angular resolution and the dynamic range at least 100. A two-parameter regression model applied for a plausible range of dependence of linear size on luminosity and redshift is used to separate the “ $\beta - n$ ” parameter space and gives a deceleration parameter somewhat lower than the critical,  $q_0 \leq 0.5$ , for  $\beta + n \gtrsim -0.15$ . Such an approach might be useful to further restrict the deceleration parameter using a better understanding of physics of the compact radio structures, represented by parameters  $\beta$  and  $n$ .

We also find a dependence of angular size with spectral index which, if not considered, increases the dispersion in linear size. Elimination of extreme values of spectral indices with  $\alpha < -0.38$  and  $\alpha > 0.18$  better defines compact sources as standard rods.

In view of the size and selection bias in the currently available sample, we have chosen not to consider more general models with  $\Lambda \neq 0$ . However, we present our full data set for those may wish to use these data to further investigate constraints on the cosmological parameters.

*Acknowledgements.* We are grateful to the referee for helpful comments. LIG acknowledges partial support from the European Union under contract No. CHGECT 920011, the Netherlands Organization for Scientific Research (NWO) programme on the Early Universe, and the European Commission, TMR Programme, Research Network Contract ERBFMRXCT 96-0034 “CERES”. SF acknowledges financial support received from the NWO and the Hungarian Space Office, and hospitality of JIVE and NFRA during his fellowship in Dwingeloo. KIK acknowledges the hospitality of JIVE during two visits. We acknowledge the use of the NASA/IPAC Extragalactic Database (NED), which is operated by the Jet Propulsion Laboratory, California Institute of Technology, under contract with the National Aeronautics and Space Administration. The National Radio Astronomy Observatory is operated by Associated Universities, Inc. under a Cooperative Agreement with the National Science Foundation.

## References

- Aller M.F., Aller H.D., Hughes P.A., 1992, ApJ 399, 16
- Alef W., Wu S.Y., Preuss E., et al., 1996, A&A 308, 376
- Barthel P.D., Miley G.K., 1988, Nature 333, 319
- Brinkman W., Siebert J., Reich W., et al., 1995, A&AS 109, 147
- Buchalter A., Helfand D.J., Becker R.H., White R.L., 1998, ApJ 494, 503
- Carilli C.L., Bartel N., Diamond P.J., 1994, AJ 108, 64
- Chu H.S., Bååth L.B., et al., 1996, A&A 307, 15
- Cawthorne T.V., Gabuzda D.C., 1996, MNRAS 278, 861
- Cawthorne T.V., Wardle J.F.C., Roberts D.H., Gabuzda D.C., Brown L.F., 1993, ApJ 416, 496
- Conway J.E., Pearson T.J., Readhead A.C.S., et al., 1992, ApJ 396, 62
- Dabrowski Y., Lasenby A., Saunders R., 1995, MNRAS 277, 753

- Downes D., Solomon P.M., Radford S.J.E., 1993, *ApJ* 414, 13L
- De Vacoulers G., De Vacoulers A., Corwin Jr. H.G., et al., 1991, *Third Reference Catalogue of Bright Galaxies*, v. 3.9
- De Waard G., 1987, Ph.D. Thesis, Leiden University
- Feretti L., Comoretto G., Giovannini G., Venturi T., Wehrle A.E., 1993, *ApJ* 408, 446
- Ficarra A., Grueff G., Tomasetti G., 1985, *A&AS* 59, 255
- Frey S., 1998, PhD Thesis, Eötvös University, Budapest, in preparation
- Frey S., Gurvits L.I., Kellermann K.I., Schilizzi R.T., Pauliny-Toth I.I.K., 1997, *A&A* 325, 511
- Gabuzda D.C., Cawthorne T.V., Roberts D.H., Wardle J.F.C., 1992, *ApJ* 388, 40
- Gabuzda D.C., Mullan C.M., Cawthorne T.V., Wardle J.F.C., Roberts D.H., 1994, *ApJ* 435, 140
- Gabuzda D.C., Wardle J.F.C., Roberts D.H., 1989, *ApJ* 336, L59
- Giovannini G., Feretti L., Venturi T., et al., 1994, *ApJ* 435, 116
- Gregory P.C., Scott W.K., Douglas K., Condon J.J., 1996, *ApJS* 103, 427
- Gregory P.C., Vavasour J.D., Scott W.K., Condon J.J., 1994, *ApJS* 90, 173
- Guirado J.C., Marcaide J.M., Elosegui P., et al., 1995, *A&A* 293, 613
- Gurvits L.I., 1993, in Davies R.D., Booth R.S. (eds.) *Sub-Arcsecond Radio Astronomy*. Cambridge Univ. Press, Cambridge, p. 380
- Gurvits L.I., 1994, *ApJ* 425, 442
- Gurvits L.I., Kardashev N.S., Popov M.V., et al., 1992, *A&A* 260, 82
- Gurvits L.I., Schilizzi R.T., Barthel P.D., et al., 1994, *A&A* 291, 737
- Henstock D.R., Browne I.W.A., Wilkinson P.N., et al., 1995, *ApJS* 100, 1
- Henstock D.R., Browne I.W.A., Wilkinson P.N., McMahon R.G., 1997, *MNRAS* 290, 380
- Herbig T., Readhead A.C.S., 1992, *ApJS* 81, 83
- Hewitt A., Burbidge G., 1991, *ApJS* 75, 297
- Hewitt A., Burbidge G., 1993, *ApJS* 87, 451
- Hong X.Y., Venturi T., Wan T.S., et al., 1998, *A&A*, in preparation
- Hooimeyer J.R.A., Schilizzi R.T., Miley G.K., Barthel P.D., 1992a, *A&A* 261, 5
- Hooimeyer J.R.A., Schilizzi R.T., Miley G.K., Barthel P.D., 1992b, *A&A* 261, 25
- Hook I.M., McMahon R.G., 1997, *MNRAS*, submitted
- Jackson J.C., Dodgson M., 1996, *MNRAS* 278, 603
- Jones D.L., Unwin S.C., Readhead A.C.S., et al., 1986, *ApJ* 305, 684
- Kapahi V.K., 1987, in Hewitt A., Burbidge G., Fang L.Z. (eds) *Observational Cosmology*. Reidel, Dordrecht, p. 251
- Kapahi V.K., 1989, *AJ* 97, 1
- Kayser R., 1995, *A&A* 294, L21
- Keel W.C., 1985, *AJ* 90, 2207
- Kellermann K.I., 1993, *Nature* 361, 134
- Krauss L.M., Schramm D.N., 1993, *ApJ* 405, L43
- Kühr H., Nauber U., Pauliny-Toth I.I.K., Witzel A., 1981a, *Max-Planck-Institut für Radioastronomie*, Pr. No. 55
- Kühr H., Pauliny-Toth I.I.K., Witzel A., Schmidt J., 1981b, *AJ* 86, 854
- Kus A.J., Wilkins P.N., Pearson T.J., Readhead A.C.S., 1990, in Zensus J.A., Pearson T.J. (eds.) *Parsec-scale Radio Jets*, Cambridge Univ. Press, Cambridge, p. 161
- Lobanov A.P., 1996, Ph.D. Thesis, New Mexico Institute of Mining and Technology, Socorro
- Marcha M.J.M., Browne I.W.A., Impey C.D., Smith P.S., 1996, *MNRAS* 281, 425
- Marscher A.P., 1988, *ApJ* 334, 552
- Marzke R.O., Huchra J.P., Geller M.J., 1996, *AJ* 112, 1803
- McHardy I.M., Marscher A.P., Gear W.R., et al., 1990, *MNRAS* 246, 305
- McMahon R.G., Hook I.M., 1998, in preparation
- Michel A., Huchra J. 1988, *PASP* 100, 1423
- Neeser M.J., Eales S.A., Law-Green J., Leahy J.P., Rawlings S., 1995, *ApJ* 451, 76
- Nilsson K., Valtonen M.J., Kotilainen J., Jaakkola T., 1993, *ApJ* 413, 453
- Oren A.L., Wolfe A.M., 1995, *ApJ* 445, 624
- Owen F.N., Ledlow M.J., Keel W.C., 1995, *AJ* 109, 140
- Paragi Z., Frey S., Gurvits L.I., et al., 1998, in preparation
- Pearson T.J., Blundell K.M., Riley J.M., Warner P.J., 1992, *MNRAS* 259, 13p
- Pearson T.J., Readhead A.C.S., 1988, *ApJ* 328, 114
- Perlman E.S., Carilli C.L., Stocke J.T., Conway J.E., 1996, *AJ* 111, 1839
- Preston R.A., Morabito D.D., Williams J.G., et al., 1985, *AJ* 90, 1599.
- Preuss E., Alef W., Wu S., et al., 1990, in Zensus J.A., Pearson T.J. (eds.) *Parsec-scale Radio Jets*, Cambridge Univ. Press, Cambridge, p. 120
- Polatidis A.G., Wilkinson P.N., Akujor C.E., 1993, in Davis R.D., Booth R.S. (eds.) *Sub-Arcsecond Radio Astronomy*, Cambridge Univ. Press, Cambridge, p. 225
- Romney J.D., Benson J.M., Dhawan V., et al., 1995, *Proc. Nat. Acad. Sci. USA* 92, 11360
- Rusk R.E., 1988, Ph.D. Dissertation, University of Toronto
- Sandage A.R., 1988, *ARA&A*, 26, 56
- Shen Z.-Q., Wan T.-S., Moran J.M., et al., 1997, *AJ* 114, 1999
- Shen Z.-Q., Wan T.-S., Moran J.M., et al., 1998, *AJ* 115, 1357
- Simon R.S., Hall J., Johnston K.J., et al., 1988, *ApJ* 326, L5
- Singal A.K., 1993, *MNRAS* 263, 139
- Snellen I.A.G., 1997, Ph.D. Thesis, Leiden University
- Snellen I.A.G., Bremer M.N., Schilizzi R.T., Miley G.K., van Ojik R., 1996, *MNRAS* 279, 1294
- Standke K.J., Quirrenbach A., Krichbaum T.P., et al., 1996, *A&A* 306, 27
- Stelmach J., 1994, *AJ* 428, 61
- Stepanas P.G., Saha P., 1995, *MNRAS* 272, L13
- Stickel M., Kühr H., 1993, *A&AS* 100, 395
- Stickel M., Kühr H., 1994 *A&AS* 105, 67
- Strauss M.A., Huchra J.P., Davis M., et al., 1992, *ApJS* 83, 29
- Taylor G.B., Vermeulen R.C., Pearson T.J., et al., 1994, *ApJS* 95, 345
- Taylor G.B., Vermeulen R.C., Readhead A.C.S., et al., 1996, *ApJS* 107, 37
- Tingay S.J., Edwards P.G., Costa M.E., et al., 1996, *ApJ* 464, 170
- Tingay S.J., Murphy D.W., Edwards P.G., 1998, *ApJ* 500, 673
- Udomprasert P.S., Taylor G.B., Pearson T.J., Roberts D.H., 1997, *ApJ* 483, L9
- Unwin S.C., Cohen M.C., Biretta J.A., Hodges M.W., Zensus J.A., 1989, *ApJ* 340, 117

- Venturi T., Castaldini C., Cotton W.D., et al., 1995, *ApJ* 454, 735
- Venturi T., Giovannini G., Feretti L., Comoretto G., Wehrle A.E., 1993a, *ApJ* 408, 81
- Venturi T., Pearson T.J., Barthel P.D., Herbig T., 1993b, *A&A* 271, 65
- Vermeulen R.C., Taylor G.B., Readhead A.C.S., Browne I.W.A., 1996, *AJ* 111, 1013
- Véron-Cetty M.P., Véron P., 1996, *A Catalog of Quasars and Active Galactic Nuclei* (7th edition), *Eso Sci. Report No.* 17
- VLA Calibrator Manual 1996, R.A.Perley and G.B.Taylor, NRAO
- Walker R.C., Benson J.M., Unwin S.C., 1987, in Zensus J.A., Pearson T.J. (eds.) *Superluminal Radio Sources*, Cambridge Univ. Press, Cambridge, p. 48
- Wehrle A.E., Cohen M.C., 1989, *ApJ* 346, L69
- Wehrle A.E., Cohen M.C., Unwin S.C., 1990, in Zensus J.A., Pearson T.J. (eds.) *Parsec-scale Radio Jets*, Cambridge Univ. Press, Cambridge, p. 49
- Wehrle A.E., Cohen M.C., Unwin S.C., et al., 1992, *ApJ* 391, 589
- White R.L., Becker R.H., 1992, *ApJS* 79, 331
- White R.L., Becker R.H., Helfand D.J., Gregg M.D., 1997, *ApJ* 475, 479, and WWW version of the FIRST survey data <http://sundog.stsci.edu/>
- Wilkinson P.N., Browne I.W.A., Alcock D., et al., 1998, in Bremer M.N., Jackson N., Pérez-Fournon I. (eds.) *Observational Cosmology with New Radio Surveys*, Kluwer Acad. Publishers, Dordrecht, p. 221
- Witzel A., Schalinski C.J., Johnston K.J., et al., 1988, *A&A* 206, 245
- Wright A., Otrupcek R., 1990, *Parkes Catalogue*, Australia Telescope National Facility
- Xu W., Lawrence C.R., Readhead A.C.S., Pearson T.J., 1994, *AJ* 108, 395
- Xu W., Readhead A.C.S., Pearson T.J., Polatidis A.G., Wilkinson P.N., 1995, *ApJS* 99, 297
- Zensus J.A., Bååth L.B., Cohen M.C., Nicolson G.D., 1988, *Nature* 334, 410
- Zhang F.J., Bååth L.B., Spencer R.E., 1994, *A&A* 281, 649

**Table 1.** The sample of sources for  $\theta - z$  studies. This table is available in electronic form at the CDS via anonymous ftp to [cdsarc.u-strasbg.fr](ftp://cdsarc.u-strasbg.fr) (130.79.128.5) or via <http://cdsweb.u-strasbg.fr/Abstract.html>

Source	Name	$z$	ID <sup>a</sup>	$S_6$ [Jy]	$S_{20}$ [Jy]	$\alpha$	$\theta^b$ [mas]	Type <sup>c</sup>	Ref $z$	Ref <sup>d</sup> $S_6$	Ref <sup>e</sup> $S_{20}$	Ref VLBI 13
1	2	3	4	5	6	7	8	9	10	11	12	13
0003+380		0.229	Q	0.57	0.60	-0.04	<2.0	J	VV96			HB95
0004+139		3.20	Q	0.12	0.19	-0.23	5.1	C	MH98			PF98
0010+405	4C 40.01	0.255	G	1.04	1.80	-0.44	<2.0	L	SK93			XR95
0014+813		3.387	Q	0.55	[f]	-0.16	4.9	C	VV96	KP81	KP81	TV94
0016+731		1.781	Q	1.58	0.86	0.49	<2.0	S	VV96			PR88
0022+390		1.946	Q	0.71	0.76	-0.05	9.8	C	VV96			XR95
0035+367		0.366	Q	0.48	0.88	-0.49	3.4	C	VV96			TV96
0035+413		1.353	Q	1.14	0.44	0.77	<0.9	S	VV96			HB95
0046+063		3.580	Q	0.21	0.22	-0.02	4.0	C	MH98			PF98
0055+301	NGC 315	0.016	G	0.91	1.59	-0.45	10.2	C	DV91			VG93
0106+013		2.107	Q	4.18	4.04	0.03	10.6	C	VV96			SW97
0108+388		0.669	G	1.34	0.41	0.95	5.1	C	HR92			PR88
0110+495		0.395	Q	0.72	0.49	0.31	8.1	C	VV96			HB95
0133+476	DA 55	0.859	Q	2.02	1.40	0.30	2.9	C	VV96			CW93
0145+386		1.440	Q	0.36	0.29	0.17	3.2	C	HB93			HB95
0151+474		1.026	Q	0.50	0.35	0.29	<1.7	L	VV96			HB95
0153+744		2.338	Q	1.59	2.09	-0.22	10.6	C	VV96			WS88
0201+365		2.912	Q	0.36	0.59	-0.40	6.8	C	VV96			HB95
0205+722		0.895	G	0.53	0.84	-0.37	3.3	C	VT96			TV94
0208-512		1.003	Q	3.30	[g]	-0.12	1.7	C	VV96	GV94	WO90	TE96
0212+735		2.367	Q	2.27	2.62	-0.12	13.1	C	VV96			PR88
0219+428		0.444	B	0.99	[h]	-0.66	5.3	C	VV96		FG85	TV96
0227+403		1.019	Q	0.41	0.44	-0.06	3.6	C	HB97			HB95
0234+285	CTD 20	1.207	Q	2.79	2.33	0.15	3.5	C	VV96			WC92
0235+164		0.940	B	1.94	2.36	-0.16	2.1	C	VV96			CB96
0243+181		3.59	Q	0.22	0.19	0.12	4.6	C	MH98			PF98
0248+430		1.310	Q	1.37	0.83	0.40	11.4	C	VV96			XR95
0249+383		1.122	Q	0.45	0.78	-0.44	6.3	C	HB97			HB95
0251+393		0.291	Q	0.35	0.30	0.12	1.6	C	VV96			HB95
0256+424		0.867	Q	0.39	0.62	-0.37	20.9	C	VV96			HB95
0307+380		0.816	Q	0.63	0.12	1.33	<1.0	J	VV96		VL96	HB95
0309+411	NRAO 128	0.134	G	0.53	0.47	0.10	3.9	C	MB96			HB95
0316+413	3C 84	0.018	G	46.89	21.20	0.64	10.2	C	SH92			RB95
0332-403		1.445	Q	2.60	1.92	0.23	2.0	C	VV96	WO90	WO90	SW98
0333+321	NRAO 140	1.259	Q	1.95	3.08	-0.37	9.8	C	VV96			Ma88
0336-019	CTA 26	0.852	Q	2.58	2.25	0.08	1.3	C	VV96	KN81		WC92
0400+258		2.109	Q	0.99	1.48	-0.32	4.4	C	VV96			Ru88
0403-132		0.571	Q	3.24	4.00	-0.17	<1.4	L	VV96	WO90	WO90	SW98
0410+110	3C 109	0.306	G	1.39	3.93	-0.84	3.5	C	HB91			GF94
0415+379	3C 111	0.049	G	5.17	13.53	-0.77	9.5	C	HB91			PA90
0420-014		0.915	Q	4.15	2.24	0.50	1.7	C	VV96	WO90	WO90	HV98
0430+052	3C 120	0.033	G	4.20	3.85	0.07	11.8	C	MH88			WB87
0444+634		0.781	Q	0.52	0.37	0.27	5.3	C	VV96			TV94
0454-234		1.003	Q	2.00	[x]	0.21	2.4	C	VV96	WO90	WO90	SW98
0454+844		0.112	B	1.40	[i]	0.38	1.3	C	VV96	KP81	KP81	WS88
0458-020		2.286	Q	2.19	2.20	0.00	4.6	C	VV96	WO90	WO90	WC92
0521-365		0.055	G	9.23	16.30	-0.46	3.9	C	Ke85	WO90	WO90	TE96
0537-441		0.896	B	3.80	2.70	0.28	3.9	C	VV96	WO90	WO90	TE96
0537+531		1.275	Q	0.67	0.66	0.01	2.3	C	VV96			TV94
0546+726		1.555	Q	0.39	0.49	-0.18	4.4	C	HB97			TV94



**Table 1.** *continued*

1	2	3	4	5	6	7	8	9	10	11	12	13
0552+398	DA 193	2.365	Q	5.52	1.75	0.92	<1.0	J	VV96			WC92
0554+580		0.904	Q	0.85	0.37	0.67	3.4	C	HB97			TV94
0600+442		1.136	Q	0.71	1.21	-0.43	10.1	C	VV96			HB95
0601+579		1.840	Q	0.16	0.14	0.11	<1.3	J	Sn97			Sn97
0609+607		2.702	Q	1.07	1.06	0.01	4.9	C	HB97			TV94
0615+820		0.71	Q	1.00	0.78	0.20	<1.0	L	VV96	KP81		XR95
0620+389		3.469	Q	0.84	1.22	-0.30	6.5	C	VV96			XR95
0627+532		2.204	Q	0.45	0.81	-0.47	10.2	C	HB97			HB95
0633+734		1.850	Q	0.71	1.10	-0.35	5.7	C	HB97			TV94
0636+680		3.177	Q	0.49	0.13	1.07	<1.5	L	VV96			TV94
0641+393		1.266	Q	0.44	0.37	0.14	3.6	C	HB97			HB95
0642+449		3.408	Q	1.22	0.60	0.57	3.1	C	VV96			XR95
0646+600		0.455	Q	0.94	0.44	0.61	3.0	C	VV96			XR95
0650+371		1.982	Q	0.87	0.59	0.31	<0.8	J	VV96			XR95
0650+453		0.933	Q	0.47	0.59	-0.18	<1.0	J	HB97			HB95
0651+410		0.022	G	0.43	0.30	0.29	<2.0	L	MH96			HB95
0707+476		1.292	Q	0.98	0.98	0.00	3.5	C	VV96			XR95
0710+439		0.518	Q	1.61	1.83	-0.10	24.0	C	VV96			CP92
0711+356		1.626	Q	0.82	1.43	-0.45	5.2	C	VV96			PR88
0714+457		0.940	Q	0.47	0.41	0.11	3.9	C	VV96			HB95
0724+571		0.426	Q	0.39	0.41	-0.04	4.3	C	HB97			TV94
0727+409		2.501	Q	0.47	0.41	0.11	4.0	C	VV96			HB95
0730+504		0.720	Q	0.99	0.39	0.75	2.5	C	HB97			TV94
0731+479		0.782	Q	0.51	0.43	0.14	3.6	C	VV96			HB95
0740+828		1.991	Q	0.93	1.82	-0.54	8.9	C	VV96	KP81		XR95
0743+744		1.629	Q	0.48	0.35	0.25	2.2	C	VV96			HB95
0746+483		1.951	Q	0.90	0.66	0.25	3.0	C	VV96			XR95
0754+100		0.66	B	0.90	1.05	-0.12	1.5	C	VV96			GC92
0755+379	NGC 2484	0.043	G	1.11	2.58	-0.68	5.6	C	DV91			XR95
0758+595		1.977	Q	0.18	0.14	0.20	2.0	C	Sn97			Sn97
0803+452		2.102	Q	0.38	0.39	-0.02	2.1	C	HB97			HB95
0804+499		1.433	Q	1.32	0.89	0.32	<1.2	S	VV96			PR88
0805+410		1.420	Q	0.69	0.36	0.52	3.0	C	VV96			XR95
0806+573		0.611	Q	0.41	0.43	-0.04	25.1	C	HB97			TV94
0812+367		1.025	Q	0.99	1.02	-0.02	10.6	C	VV96			XR95
0820+560		1.417	Q	1.16	1.27	-0.07	2.7	C	VV96			XR95
0821+394		1.216	Q	1.03	1.38	-0.24	4.3	C	VV96			XR95
0821+621		0.542	Q	0.62	0.65	-0.04	32.6	C	VV96			TV94
0824+355		2.249	Q	0.75	0.87	-0.12	<1.0	J	VV96			HB95
0826+707		2.003	Q	0.11	0.07	0.36	<1.3	J	Sn97		Sn97	Sn97
0828+493		0.548	B	0.37	1.00	-0.80	2.2	C	VV96			XR95
0830+102		3.750	Q	0.13	0.15	-0.11	14.2	C	OW95			PF98
0830+425		0.253	Q	0.39	0.24	0.39	4.7	C	HB97		WB97	HB95
0831+557	4C 55.16	0.242	G	5.74	7.74	-0.24	5.3	C	AA92			PR88
0833+416		1.298	Q	0.39	0.43	-0.08	4.0	C	HB97			HB95
0833+585		2.101	Q	0.72	0.60	0.15	1.2	C	VV96			XR95
0836+290	4C 29.30	0.079	G	0.27	0.88	-0.95	6.3	C	OL95			VC95
0836+710		2.172	Q	2.34	4.24	-0.48	8.7	C	VV96			WS88
0850+581	4C 58.17	1.322	Q	1.18	1.42	-0.15	6.0	C	VV96			HS92
0851+202	OJ287	0.306	Q	2.91	2.28	0.20	3.0	C	VV96			GW89

**Table 1.** *continued*

1	2	3	4	5	6	7	8	9	10	11	12	13
0859+681		1.499	Q	0.66	0.59	0.09	4.9	C	VV96			TV94
0900+520		1.537	Q	0.37	0.32	0.12	1.4	C	HB97			TV94
0902+490		2.690	Q	0.55	0.64	-0.12	<1.0	S	VV96			HB95
0906+041		3.20	Q	0.13	0.21	-0.38	7.1	C	BS95			PF98
0906+430	3C 216	0.668	Q	1.61	4.27	-0.79	3.5	C	VV96			VP93
0913+391		1.269	Q	0.55	1.06	-0.53	3.4	C	VV96			HB95
0917+449		2.180	Q	1.09	0.78	0.27	2.8	C	VV96			XR95
0917+624		1.446	Q	1.23	1.23	0.00	5.1	C	VV96			SQ96
0923+392	4C 39.25	0.698	Q	6.91	2.72	0.75	2.0	C	VV96			PR88
0929+533		0.595	Q	0.39	0.54	-0.26	5.6	C	VV96			TV94
0930+493		2.582	Q	0.53	0.73	-0.26	2.3	C	HB97			HB95
0933+503		0.276	G	0.32	0.14	0.67	<1.0	J	HB97		VL96	HB95
0938+119		3.191	Q	0.12	0.29	-0.70	2.8	C	VV96			PF98
0941+522		0.565	Q	0.39	0.85	-0.63	6.8	C	VV96			HB95
0945+408	4C 40.24	1.252	Q	1.80	1.49	0.15	8.3	C	VV96			PR88
0949+354		1.875	Q	0.37	0.34	0.07	8.5	C	VV96			HB95
0954+658		0.367	Q	1.13	0.65	0.45	1.8	C	VV96			GM94
0955+476		1.873	Q	1.01	0.69	0.31	<1.8	J	VV96			XR95
1003+830		0.322	G	0.72	0.60	0.15	6.0	C	XL94	KP81		XR95
1010+350		1.414	Q	0.63	0.42	0.33	8.1	C	VV96			HB95
1020+400		1.254	Q	0.79	1.16	-0.31	3.4	C	VV96			XR95
1030+398		1.095	Q	0.65	0.38	0.43	2.0	C	VV96			HB95
1030+415		1.120	Q	0.44	0.77	-0.45	4.2	C	VV96			XR95
1030+611		0.336	G	0.53	0.77	-0.30	3.8	C	VV96			TV94
1034-293		0.312	B	1.51	[j]	0.21	<1.3	L	VV96	WO90	WO90	HV98
1038+528		0.677	Q	0.70	0.71	-0.01	<1.5	J	VV96			HB95
1039+811		1.256	Q	1.14	0.73	0.36	2.3	C	VV96	KP81		XR95
1041+536		1.897	Q	0.44	0.54	-0.16	3.3	C	HB97			HB95
1044+719		1.15	Q	1.90	0.62	0.90	<1.5	L	VV96			XR95
1053+704		2.492	Q	0.54	0.61	-0.10	1.9	C	VV96			XR95
1053+815		0.706	G	0.77	0.34	0.66	<1.5	J	XL94	KP81		XR95
1055+201		1.11	Q	1.51	2.31	-0.34	<2.0	L	VV96			HS92
1058+726		1.46	Q	0.86	1.45	-0.42	19.2	C	VV96			XR95
1058+629		0.664	Q	0.69	0.60	0.11	1.4	C	HB97			XR95
1101+384	Mrk421	0.031	B	0.72	0.84	-0.12	12.8	C	VV96			XR95
1104-445		1.598	Q	2.03	1.92	0.04	2.7	C	VV96	WO90	WO90	SW97
1105+437		1.226	Q	0.34	0.27	0.19	1.6	C	HB97			HB95
1124+571		2.890	Q	0.45	0.78	-0.44	2.0	C	VV96			TA94
1127-145		1.187	Q	5.46	6.40	-0.13	16.1	C	VV96	WO90	WO90	WC92
1128+385		1.733	Q	0.77	0.93	-0.15	<1.0	J	VV96			XR95
1143+590		1.982	Q	0.58	0.28	0.59	<1.1	J	HB97			TV94
1144+352		0.063	G	0.67	0.70	-0.04	21.6	C	MB96			HB95
1144+542		2.201	Q	0.52	0.41	0.19	2.5	C	VV96			XR95
1146+531		1.629	Q	0.29	0.20	0.30	1.5	C	VV96		VL96	HB95
1146+596	NGC 3894	0.011	G	0.57	0.41	0.27	19.9	C	DV91			TA94
1150+497	4C 49.22	0.334	Q	0.72	1.43	-0.55	<1.8	J	VV96			XR95
1150+812		1.25	Q	1.18	1.38	-0.13	2.8	C	VV96	KP81		XR95
1151+408		0.916	Q	0.37	0.70	-0.51	1.7	C	HB97			HB95
1155+486		2.028	Q	0.55	0.48	0.11	2.2	C	HB97			HB95
1156+295		0.729	Q	1.46	1.75	-0.15	3.6	C	VV96			MM90

**Table 1.** *continued*

1	2	3	4	5	6	7	8	9	10	11	12	13
1213+350		0.857	Q	1.12	1.73	-0.35	36.8	C	VV96			XR95
1214+588		2.547	Q	0.31	0.42	-0.24	2.0	C	HB97			TV94
1216+487		1.076	Q	0.64	0.86	-0.24	5.8	C	VV96			XR95
1222+216		0.435	Q	1.15	1.97	-0.43	3.4	C	VV96			HO92
1223+395		0.623	Q	0.51	0.54	-0.05	17.4	C	VV96			HB95
1225+368		1.975	Q	0.79	2.14	-0.80	31.3	C	VV96			XR95
1226+023	3C 273	0.158	Q	43.57	50.10	-0.11	26.1	C	VV96			ZB88
1226+373		1.515	Q	0.86	0.19	1.22	<0.9	J	HB97			HB95
1239+376		3.818	Q	0.37	0.54	-0.30	<2.0	L	VT96			HB95
1240+381		1.316	Q	0.76	0.36	0.60	<1.0	J	VV96			HB95
1244-255		0.638	Q	1.55	[y]	0.24	<1.6	L	VV96	WO90	WO90	SW98
1253-055	3C 279	0.538	Q	13.00	11.60	0.09	3.2	C	VV96	WO90	WO90	UC89
1254+571		0.042	G	0.42	0.29	0.30	<1.5	J	DS93			TV94
1258+507		1.561	Q	0.44	0.52	-0.13	<1.5	J	VV96			HB95
1305+804		1.183	Q	0.38	0.86	-0.66	13.3	C	VT96	KP81		TV96
1307+562		1.629	Q	0.42	0.29	0.30	1.9	C	HB97			TV94
1308+326		0.997	Q	1.45	1.61	-0.08	3.8	C	VV96			GC92
1309+555		0.926	Q	0.68	0.21	0.95	<1.4	J	HB97			TV94
1311+552		0.613	Q	0.55	1.17	-0.61	38.4	C	VT96			TV94
1317+520		1.055	Q	0.61	1.29	-0.60	8.7	C	VV96			HS92
1321+410		0.496	Q	0.41	0.36	0.10	5.4	C	VT96			HB95
1323+800		1.970	Q	0.46	[k]	0.22	3.5	C	VV96	KP81	KP81	TV94
1325+436		2.073	Q	0.58	0.70	-0.15	<1.0	J	VV96			HB95
1333+459		2.450	Q	0.65	0.31	0.60	<1.0	J	VV96			XR95
1334-127		0.539	Q	4.30	1.90	0.66	1.6	C	VV96	VL96	VL96	HV98
1335+552		1.096	Q	0.75	0.72	0.03	2.1	C	VV96			TV94
1337+637		2.558	Q	0.42	0.50	-0.14	7.0	C	VV96			TV94
1338+381		3.103	Q	0.26	0.33	-0.11	3.8	C	VV96			PF98
1342+662		0.766	Q	0.30	0.89	-0.88	<1.2	J	VV96			TV94
1342+663		1.351	Q	0.55	0.89	-0.39	<1.3	L	VV96			XR95
1347+539		0.976	Q	0.64	1.15	-0.47	12.8	C	VV96			XR95
1354-174		3.147	Q	0.97	1.90	-0.54	<1.9	J	VV96	WO90	WO90	FG97
1354+195		0.719	Q	2.62	2.63	0.00	12.3	C	VV96			Ru88
1356+478		0.230	G	0.43	0.59	-0.25	6.0	C	VT96			TV96
1402+044		3.211	Q	1.00	0.56	0.47	14.5	C	VV96			GK92
1404+286	OQ208	0.077	G	2.35	0.76	0.91	6.9	C	VV96			ZB94
1413+135		0.247	B	0.85	1.21	-0.28	34.8	C	VV96			PC96
1413+373		2.36	Q	0.38	0.37	0.02	4.0	C	VV96			HB95
1415+463		1.552	Q	0.80	1.01	-0.19	10.5	C	VV96			HB95
1417+385		1.832	Q	0.65	0.71	-0.07	<0.9	S	VV96			HB95
1418+546		0.152	B	1.35	1.56	-0.12	3.8	C	VV96			XR95
1421+482		2.220	Q	0.52	0.36	0.30	2.9	C	VV96			HB95
1424+366		1.091	Q	0.44	0.19	0.68	<0.9	J	HB97			HB95
1427+543		2.991	Q	0.72	0.90	-0.18	9.8	C	HB97			HB95
1428+422		4.715	Q	0.34	0.31	0.07	<1.2	L	HM97			PF98
1432+422		1.240	Q	0.35	0.28	0.18	<1.6	J	VT96			TV96
1435+638		2.062	Q	0.76	1.39	-0.49	8.9	C	VV96			XR95
1438+385		1.775	Q	0.89	1.03	-0.12	8.8	C	VT96			XR95
1442+101		3.535	Q	1.28	2.42	-0.51	13.5	C	VV96			UT97
1442+637		1.380	Q	0.44	0.68	-0.35	8.7	C	VV96			TV94

**Table 1.** *continued*

1	2	3	4	5	6	7	8	9	10	11	12	13
1448+762		0.899	Q	0.68	[l]	0.32	1.9	C	VV96	KP81	KP81	HB95
1456+375		0.333	G	0.54	0.34	0.37	<1.0	J	VT96			HB95
1458+718	3C 309.1	0.904	Q	3.57	7.68	-0.62	49.8	C	VV96			KW90
1500+045		3.67	Q	0.18	0.12	0.32	0.7	C	VV96			PF98
1504-166		0.876	Q	1.96	2.70	-0.25	1.7	C	VV96	WO90	WO90	HV98
1504+377		0.674	G	0.97	1.19	-0.16	10.7	C	SK94			XR95
1505+428		0.587	Q	0.41	0.44	-0.06	5.5	C	VV96			HB95
1531+722		0.899	Q	0.44	0.66	-0.33	2.2	C	VV96			TV94
1532+016		1.435	Q	0.79	1.20	-0.33	1.2	C	VV96	WO90	WO90	HV98
1534+501		1.119	Q	0.37	0.23	0.38	<1.8	L	VV96			HB95
1538+149		0.605	B	1.21	1.45	-0.15	4.5	C	VV96			GC92
1538+593		3.878	Q	0.08	0.05	0.38	<1.1	J	Sn97		Sn97	Sn97
1543+480		1.277	Q	0.44	0.67	-0.34	34.6	C	VV96			HB95
1543+517		1.924	Q	0.59	0.49	0.15	5.1	C	HB97			HB95
1547+507		2.169	Q	0.73	0.67	0.07	7.1	C	VV96			XR95
1550+582		1.319	Q	0.35	0.23	0.34	<1.4	J	HB97			HB95
1557+031		3.891	Q	0.41	0.48	-0.13	<1.2	L	VV96			PF98
1602+576		2.858	Q	0.37	0.79	-0.61	3.9	C	VV96			HB95
1614+051		3.217	Q	0.92	0.31	0.88	<1.0	S	VV96			GK92
1619+491		1.513	Q	0.44	0.47	-0.05	10.9	C	HB97			HB95
1622-297		0.815	Q	1.86	2.20	-0.13	16.0	C	VV96	WO90	WO90	TM98
1622+665		0.203	Q	0.52	0.20	0.77	<2.0	J	VV96			TV96
1623+578		0.789	G	0.59	0.50	0.13	3.1	C	VT96			TV96
1624+416	4C 41.32	2.55	Q	1.25	1.68	-0.24	5.4	C	VV96			PR88
1626+396	3C 338	0.030	G	0.46	3.71	-1.68	11.5	C	DV91			FC93
1633+382		1.814	Q	3.22	1.90	0.42	1.7	C	VV96			PR88
1636+473		0.740	Q	1.24	0.95	0.21	<1.9	J	VV96			HB95
1637+826	NGC 6251	0.023	G	0.70	0.40	0.45	5.0	C	DV91	VL96	VL96	JU86
1638+398		1.666	Q	1.12	0.66	0.43	<0.9	J	VV96			XR95
1638+540		1.977	Q	0.35	0.31	0.10	2.7	C	HB97			HB95
1641+399	3C 345	0.594	Q	8.72	7.89	0.08	5.6	C	VV96			Lo96
1642+690	4C 69.21	0.751	Q	1.53	1.51	0.01	4.1	C	VV96			PR88
1645+410		0.835	Q	0.40	0.32	0.18	<2.1	J	HB97			HB95
1645+635		2.379	Q	0.48	0.30	0.38	7.4	C	HB97			TV94
1652+398	Mrk501	0.034	G	1.38	1.44	-0.03	7.8	C	DV91			PR88
1656+477		1.622	Q	1.24	0.78	0.37	5.7	C	VV96			XR95
1656+571		1.290	Q	0.76	0.81	-0.05	4.4	C	VV96			TV94
1700+685		0.301	Q	0.38	0.30	0.19	2.0	C	HB97			TV94
1716+686		0.777	Q	0.84	0.41	0.58	1.7	C	VV96			TV94
1719+357		0.263	Q	0.78	0.84	-0.06	4.1	C	VV96			XR95
1722+401		1.049	Q	0.52	0.55	-0.05	4.5	C	VT96			HB95
1726+455		0.714	Q	0.94	0.43	0.63	<0.9	J	VV96			HB95
1730-130	NRAO 530	0.902	Q	4.10	5.20	-0.19	4.5	C	VV96	WO90	WO90	SW97
1732+389		0.976	Q	0.56	0.78	-0.27	<0.9	J	VV96			XR95
1738+476		0.316	B	0.82	0.83	-0.01	<0.9	J	VV96			XR95
1738+499		1.545	Q	0.43	0.57	-0.23	<1.6	J	VV96			TV94
1739+522		1.379	Q	1.70	1.98	-0.12	<0.7	J	VV96			PR88
1741-038		1.057	Q	2.30	1.17	0.53	1.6	L	VV96	WO90	WO90	SW97
1743+173		1.702	Q	0.69	1.36	-0.55	9.0	C	VV96			Ru88
1745+624		3.889	Q	0.59	0.76	-0.20	2.7	C	VV96			TV94

**Table 1.** *continued*

1	2	3	4	5	6	7	8	9	10	11	12	13
1746+693		1.886	Q	0.14	0.20	-0.28	1.7	C	Sn97			Sn97
1749+096		0.320	Q	2.46	0.61	1.12	1.7	C	VV96			WC92
1749+701		0.770	Q	0.72	1.31	-0.48	4.7	C	VV96			GM94
1751+441		0.871	Q	1.00	0.78	0.20	1.7	C	VV96			XR95
1755+578		2.110	Q	0.46	0.73	-0.37	10.8	C	HB97			TV94
1758+388		2.092	Q	0.74	0.51	0.30	1.4	C	VV96			XR95
1800+440		0.663	Q	1.19	0.88	0.24	<0.9	J	VV96			XR95
1803+784		0.684	Q	2.63	1.87	0.27	1.6	C	VV96	KP81		CW93
1806+456		0.830	Q	0.35	0.15	0.68	<1.7	J	VV96			TV94
1807+698	3C 371	0.051	Q	2.12	2.26	-0.05	4.0	C	VV96			CW93
1811+430		1.090	Q	0.51	0.97	-0.52	10.9	C	VV96			TV94
1812+412		1.564	Q	0.52	0.64	-0.17	10.1	C	HB97			HB95
1818+356		0.971	Q	0.57	0.99	-0.44	<1.6	J	VT96			TV96
1823+568		0.664	B	1.26	1.48	-0.13	6.1	C	VV96			GM94
1826+796		0.224	Q	0.58	[m]	0.40	15.7	C	HB97	KP81	KP81	TV94
1828+487	3C 380	0.692	Q	5.52	14.65	-0.79	23.4	C	VV96			PW93
1830+285		0.594	Q	0.98	1.81	-0.49	1.7	C	VV96			HS92
1834+612		2.274	Q	0.57	0.45	0.19	3.0	C	HB97			TV94
1839+389		3.095	Q	0.42	[n]	0.44	<0.9	J	VT96		FG85	HB95
1841+672		0.470	G	0.16	0.15	0.05	6.4	C	SB96			Sn97
1842+681		0.475	Q	0.93	0.61	0.34	1.9	C	VV96			XR95
1843+356		0.764	G	0.79	1.03	-0.21	10.3	C	VT96			XR95
1845+797	3C 390.3	0.056	G	4.41	11.23	-0.75	4.9	C	HB91	KN81		AW96
1849+670		0.657	Q	0.85	0.90	-0.05	2.6	C	VV96			TV94
1850+402		2.12	Q	0.53	0.55	-0.03	2.4	C	VV96			HB95
1851+488		1.250	Q	0.31	0.29	0.05	<1.6	L	VT96			TV94
1856+737		0.460	Q	0.58	0.56	0.03	6.6	C	VV96			TV94
1901+319	3C 395	0.635	Q	1.86	2.95	-0.37	15.7	C	VV96			SH88
1908+484		0.513	Q	0.50	0.58	-0.12	<1.6	J	HB97			TV94
1910+375		1.104	Q	0.41	0.50	-0.16	<2.3	J	HB97			HB95
1915+657		0.486	Q	0.35	0.77	-0.63	32.6	C	HB97			HB95
1921-293		0.352	Q	10.60	5.70	0.49	6.7	C	VV96	WO90	WO90	SW97
1924+507		1.098	Q	0.35	0.66	-0.51	2.1	C	VV96			HB95
1928+738		0.303	Q	3.63	3.91	-0.06	8.4	C	VV96			GM95
1936+714		1.864	Q	0.40	0.62	-0.35	<1.1	J	VV96			TV94
1943+546		0.263	G	0.94	1.65	-0.45	40.9	C	SK93			XR95
1945+604		2.700	Q	0.08	0.06	0.23	<1.0	J	Sn97		Sn97	Sn97
1946+708		0.101	G	0.68	0.92	-0.24	33.2	C	SK93			TV94
1950+573		0.652	Q	0.51	0.57	-0.09	13.5	C	HB97			TV94
1954-388		0.630	Q	2.00	1.59	0.18	<2.1	L	VV96	WO90	WO90	SW98
1957+405	Cyg A	0.056	G	0.74 <sup>q</sup>	0.78 <sup>q</sup>	-0.04	15.4	C	VV96	CB94	CB94	CB94
1958+619		1.824	Q	0.14	0.11	0.19	<1.1	J	Sn97		Sn97	Sn97
2005+642		1.574	Q	0.72	0.17	1.16	<1.1	J	HB97			TV94
2007+659		1.325	Q	0.75	1.03	-0.26	2.3	C	VV96			TV94
2007+777		0.342	B	1.28	0.94	0.25	3.6	C	VV96	KP81		GM94
2015+657		2.845	Q	0.53	0.97	-0.49	<1.2	J	VV96			TV94
2017+745		2.187	Q	0.54	0.47	0.11	4.9	C	HB97			TV94
2021+614		0.227	G	2.62	2.13	0.17	9.1	C	VV96			PR88
2043+749	4C 74.26	0.104	Q	0.37	1.60	-1.18	2.6	C	VV96			PB92
2048+312		3.198	Q	0.59	0.75	-0.19	2.8	C	VV96		VL96	GS94

**Table 1.** *continued*

1	2	3	4	5	6	7	8	9	10	11	12	13
2116+818		0.084	G	0.38	0.54	−0.28	4.7	C	MB96	KP81		TV96
2121+053		1.941	Q	2.78	1.14	0.72	<1.0	L	VV96			WC92
2134+004		1.932	Q	9.96	3.13	0.91	4.0	C	VV96	WO90	WO90	SW97
2136+141		2.427	Q	1.07	1.15	−0.06	2.9	C	VV96			WC92
2136+824		2.357	Q	0.51	1.01	−0.55	13.7	C	HB97	KP81		TV94
2145+067		0.999	Q	4.14	2.88	0.29	7.2	C	VV96			WC92
2155−152		0.672	Q	1.58	1.26	0.18	5.4	C	VV96	WO90	WO90	SW90
2200+420	BL Lac	0.069	B	2.94	4.69	−0.38	7.0	C	VV96			PR88
2201+315		0.298	Q	2.81	1.98	0.28	5.4	C	VV96			DW87
2207+374		1.493	Q	0.86	1.71	−0.55	55.6	C	VV96			XR95
2223−052	3C 446	1.404	Q	4.51	6.37	−0.26	4.9	C	VV96	KN81		WC90
2230+114	CTA 102	1.037	Q	3.97	6.63	−0.41	15.7	C	VV96			WC89
2235+731		1.345	Q	0.39	0.30	0.21	2.6	C	VV96			TV94
2243−123		0.630	Q	2.38	[o]	−0.22	1.8	C	VV96	WO90	WO90	HV98
2246+370		1.541	Q	0.43	0.91	−0.60	<0.9	J	VT96			TV94
2251+134		0.677	Q	0.88	1.44	−0.40	1.4	C	VV96			HS92
2251+158	3C 454.3	0.859	Q	14.47	13.90	0.03	7.8	C	VV96			CG96
2253+417		1.476	Q	1.08	1.41	−0.21	4.1	C	VV96			XR95
2255+417	4C 41.45	2.150	Q	1.10	1.87	−0.43	43.5	C	VT96			XR95
2259+371		2.179	Q	0.44	0.60	−0.25	6.2	C	HB97			TV94
2309+454		1.447	Q	0.50	0.31	0.38	2.0	C	VV96			TV94
2310+385		2.181	Q	0.53	0.69	−0.21	4.4	C	HB97			HB95
2330+387		0.319	Q	0.43	0.84	−0.54	46.2	C	VV96			HB95
2335+267	3C 465	0.029	G	1.56	7.46	−1.26	8.1	C	DV91			VC95
2345−167		0.576	Q	3.47	1.20	0.85	2.5	C	VV96	WO90	WO90	HV98
2351−154		2.675	Q	0.93	[p]	−0.24	<1.2	L	VV96	WO90	WO90	HV98
2352+495		0.237	G	1.60	2.34	−0.31	32.8	C	CP92			CP92
2353+816		1.344	B	0.48	0.40	0.15	1.7	C	VT96	KP81		TV94
2355−534		1.006	Q	1.66	1.22	0.24	4.9	C	VV96	WO90	WO90	SW98
2356+390		1.201	Q	0.36	0.43	−0.14	8.8	C	HB97			HB95

<sup>a</sup> Optical counterpart: Q – quasar, B – BL Lac object, G – radio galaxy (including Seyfert galaxies of all types).

<sup>b</sup> Characteristic angular size (case C) or its upper limit (cases J, L, and S).

<sup>c</sup> Radio structure code:

- C – size between the core and the most distant 2%-component;
- J – upper limit of  $\theta$  along jet direction;
- L – upper limit of  $\theta$  along major axis of the beam;
- S – upper limit of  $\theta$  along minor axis of the beam.

<sup>d</sup> 6 cm flux density from Gregory et al. (1996) unless otherwise stated.

<sup>e</sup> Flux density from White and Becker (1992) unless otherwise stated, at 20 cm or at an alternative wavelength as stated in footnotes [f – y].

<sup>f</sup> Spectral index calculated using  $S_{11} = 0.61$  Jy.

<sup>g</sup> Spectral index calculated using  $S_{11} = 3.56$  Jy.

<sup>h</sup> Spectral index calculated using  $S_{75} = 5.05$  Jy.

<sup>i</sup> Spectral index calculated using  $S_{11} = 1.10$  Jy.

<sup>j</sup> Spectral index calculated using  $S_{11} = 1.33$  Jy.

<sup>k</sup> Spectral index calculated using  $S_{11} = 0.40$  Jy.

<sup>l</sup> Spectral index calculated using  $S_{11} = 0.56$  Jy.

<sup>m</sup> Spectral index calculated using  $S_{11} = 0.45$  Jy.

<sup>n</sup> Spectral index calculated using  $S_{75} = 0.14$  Jy.

<sup>o</sup> Spectral index calculated using  $S_{11} = 2.74$  Jy.

<sup>p</sup> Spectral index calculated using  $S_{11} = 1.08$  Jy.

<sup>q</sup>  $S_6$  and  $S_{20}$  values for the compact core component.

<sup>x</sup> Spectral index calculated using  $S_{11} = 1.76$  Jy.

<sup>y</sup> Spectral index calculated using  $S_{11} = 1.34$  Jy.

**Table 1.** *continued*: List of references.

AA92 – Aller et al. 1992	AW96 – Alef et al. 1996	BS95 – Brinkman et al. 1995
CB94 – Carilli et al. 1994	CB96 – Chu et al. 1996	CG96 – Cawthorne and Gabuzda 1996
CP92 – Conway et al. 1992	CW93 – Cawthorne et al. 1993	DS93 – Downes et al. 1993
DV91 – De Vacoulers G. et al. 1991	DW87 – De Waard G. 1987	FC93 – Feretti et al. 1993
FG85 – Ficarra et al. 1985	FG97 – Frey et al. 1997	GC92 – Gabuzda et al. 1992
GF94 – Giovannini et al. 1994	GK92 – Gurvits et al. 1992	GM94 – Gabuzda et al. 1994
GM95 – Guirado et al. 1995	GS94 – Gurvits et al. 1994	GV94 – Gregory et al. 1994
GW89 – Gabuzda et al. 1989	HB91 – Hewitt and Burbidge 1991	HB93 – Hewitt and Burbidge 1993
HB95 – Henstock et al. 1995	HB97 – Henstock et al. 1997	HM97 – Hook and McMahon 1997
HO92 – Hooimeyer et al. 1992a	HR92 – Herbig and Readhead 1992	HS92 – Hooimeyer et al. 1992b
HV98 – Hong et al. 1998	JU86 – Jones et al. 1986	Ke85 – Keel 1985
KN81 – Kühr et al. 1981a	KP81 – Kühr et al. 1981b	KW90 – Kus et al. 1990
Lo96 – Lobanov 1996	Ma88 – Marscher 1988	MB96 – Marcha et al. 1996
MH88 – Michel and Huchra 1988	MH96 – Marzke et al. 1996	MH98 – McMahon and Hook 1998
MM90 – McHardy et al. 1990	OL95 – Owen et al. 1995	OW95 – Oren and Wolfe 1995
PA90 – Preuss et al. 1990	PB92 – Pearson et al. 1992	PC96 – Perlman et al. 1996
PF98 – Paragi et al. 1998	PR88 – Pearson and Readhead 1988	PW93 – Polatidis et al. 1993
RB95 – Romney et al. 1995	Ru88 – Rusk 1988	SB96 – Snellen et al. 1996
SH88 – Simon et al. 1988	SH92 – Strauss et al. 1992	SK93 – Stickel and Kühr 1993
SK94 – Stickel and Kühr 1994	Sn97 – Snellen 1997	SQ96 – Standke et al. 1996
SW97 – Shen et al. 1997	SW98 – Shen et al. 1998	TE96 – Tingay et al. 1996
TM98 – Tingay et al. 1998	TV94 – Taylor et al. 1994	TV96 – Taylor et al. 1996
UC89 – Unwin et al. 1989	UT97 – Udomprasert et al. 1997	VC95 – Venturi et al. 1995
VG93 – Venturi et al. 1993a	VL96 – VLA Calibrator Manual 1996	VP93 – Venturi et al. 1993b
VT96 – Vermeulen et al. 1996	VV96 – Veron-Cetty and Veron 1996	WB87 – Walker et al. 1987
WB97 – White et al. 1997	WC89 – Wehrle and Cohen 1989	WC90 – Wehrle et al. 1990
WC92 – Wehrle et al. 1992	WO90 – Wright and Otrupcek 1990	WS88 – Witzel et al. 1988
XL94 – Xu et al. 1994	XR95 – Xu et al. 1995	ZB88 – Zensus et al. 1988
ZB94 – Zhang et al. 1994		

**Table 2.** Two-parameter ( $lh$  and  $q_0$ ) regression model results with  $1\sigma$  errors for different fixed values of  $\beta$  and  $n$  for the sample of 145 sources ( $Lh^2 \leq 10^{26}$  W/Hz,  $-0.38 \leq \alpha \leq 0.18$ ).

$n$		$\beta=-0.20$	$\beta=-0.10$	$\beta=-0.05$	$\beta=0.0$	$\beta=0.05$	$\beta=0.10$	$\beta=0.20$
-0.3	$lh$ (pc)	13.98±4.71	16.48±4.82	17.56±5.22	18.48±6.79	19.20±9.09	19.90±1.81	20.84±2.54
	$q_0$	<b>1.78±0.83</b>	<b>1.04±0.51</b>	<b>0.81±0.51</b>	<b>0.64±0.73</b>	<b>0.51±1.59</b>	<b>0.41±0.27</b>	<b>0.26±0.06</b>
-0.2	$lh$ (pc)	14.64±4.03	16.76±4.14	17.68±4.50	18.42±6.07	19.00±4.02	19.60±1.93	20.28±2.44
	$q_0$	<b>1.22±0.43</b>	<b>0.73±0.30</b>	<b>0.57±0.32</b>	<b>0.45±0.53</b>	<b>0.36±0.71</b>	<b>0.28±0.15</b>	<b>0.17±0.03</b>
-0.1	$lh$ (pc)	15.02±3.48	16.82±3.58	17.58±3.87	18.16±5.42	18.70±2.06	19.00±1.98	19.60±2.30
	$q_0$	<b>0.86±0.23</b>	<b>0.52±0.18</b>	<b>0.40±0.20</b>	<b>0.31±0.40</b>	<b>0.24±0.33</b>	<b>0.19±0.09</b>	<b>0.10±0.02</b>
0.0	$lh$ (pc)	15.15±3.04	16.68±3.12	17.22±3.36	17.72±4.83	18.10±1.62	18.33±1.95	18.66±2.14
	$q_0$	<b>0.60±0.13</b>	<b>0.36±0.11</b>	<b>0.28±0.13</b>	<b>0.21±0.30</b>	<b>0.16±0.18</b>	<b>0.12±0.05</b>	<b>0.05±0.01</b>
0.1	$lh$ (pc)	15.14±2.69	16.36±2.74	16.80±2.92	17.14±4.30	17.30±1.56	17.56±1.89	17.68±1.99
	$q_0$	<b>0.42±0.08</b>	<b>0.25±0.07</b>	<b>0.19±0.09</b>	<b>0.14±0.23</b>	<b>0.10±0.11</b>	<b>0.07±0.03</b>	<b>0.01±0.01</b>
0.2	$lh$ (pc)	14.92±2.40	15.88±2.43	16.20±2.56	16.46±3.81	16.60±1.55	16.74±1.79	16.24±2.05
	$q_0$	<b>0.29±0.05</b>	<b>0.16±0.05</b>	<b>0.12±0.06</b>	<b>0.08±0.18</b>	<b>0.05±0.07</b>	<b>0.02±0.02</b>	<b>2e-6±1e-3</b>
0.3	$lh$ (pc)	14.52±2.16	15.30±2.16	15.54±2.26	15.69±3.38	15.80±1.53	15.40±1.65	14.63±1.29
	$q_0$	<b>0.20±0.03</b>	<b>0.10±0.03</b>	<b>0.06±0.04</b>	<b>0.03±0.15</b>	<b>7e-3±0.04</b>	<b>5e-3±0.02</b>	<b>1e-7±1e-6</b>

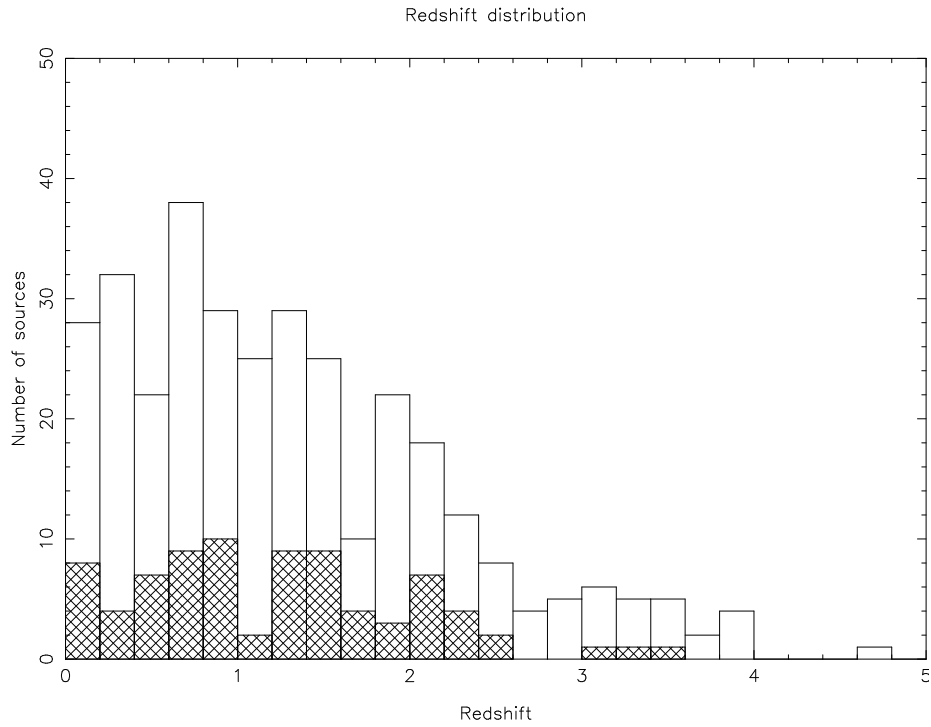


**Fig. 1.** Redshift distribution for the full sample of 330 sources. Shaded part of the histogram represents the 79 sources from Kellermann (1993).

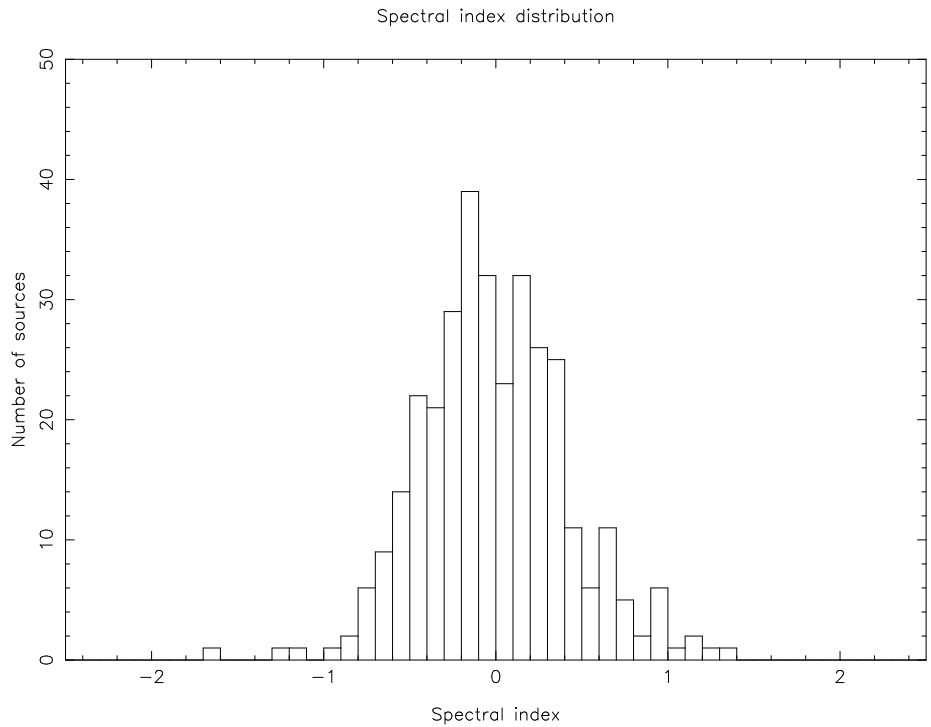


**Fig. 2.** Spectral index distribution for the sample of 330 sources ( $S \propto \nu^\alpha$ ).



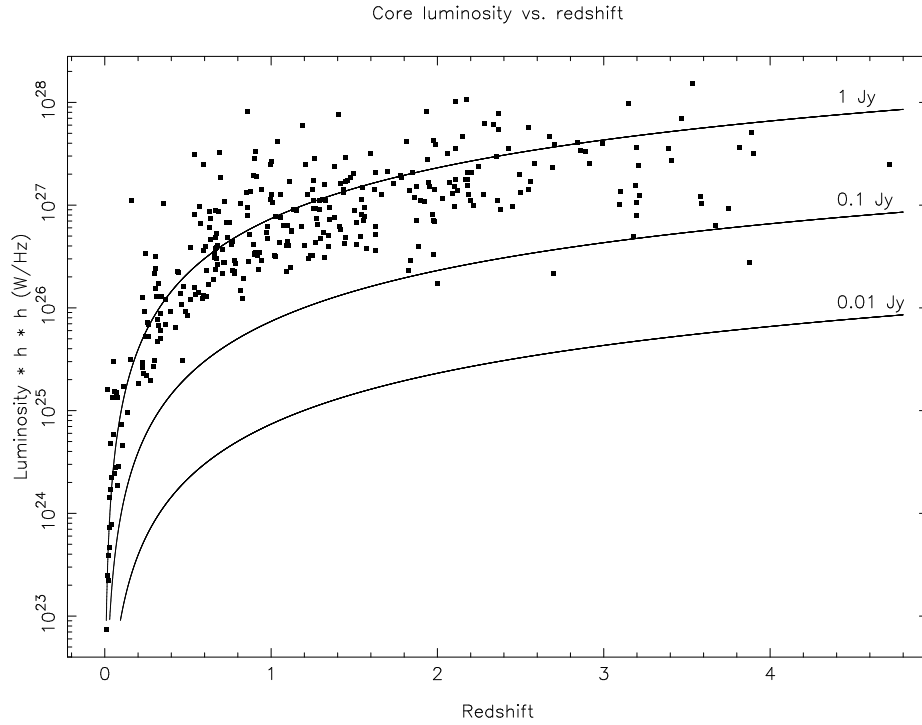


**Fig. 3.** Luminosity as a function of redshift for the full sample of 330 sources (shown by filled squares) calculated with  $H_0 = 100 h \text{ km s}^{-1} \text{ Mpc}^{-1}$  and  $q_0 = 0.5$  as a numerical example. The latter values have not been used in the regression analysis described in subsection 4.2. The solid lines show luminosities of sources with flux density of 1, 0.1 and 0.01 Jy, calculated under assumption that the spectral index  $\alpha = 0$ .

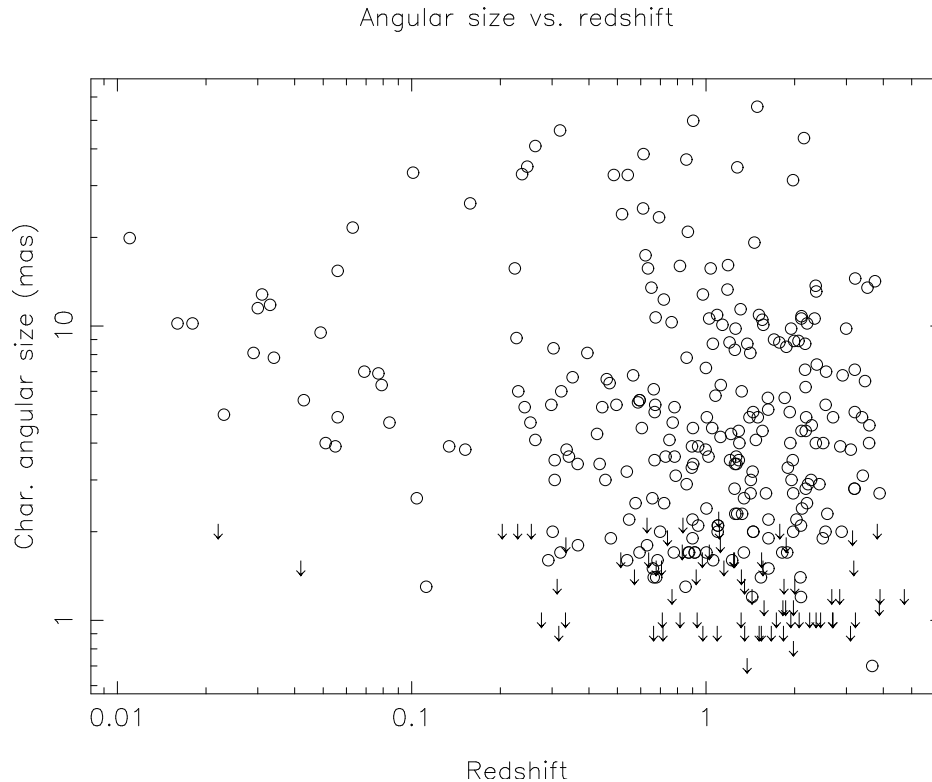


**Fig. 4.** “Angular size – redshift” diagram for the sample of 330 sources. Measured sizes are shown with empty circles, upper limits – with arrows.

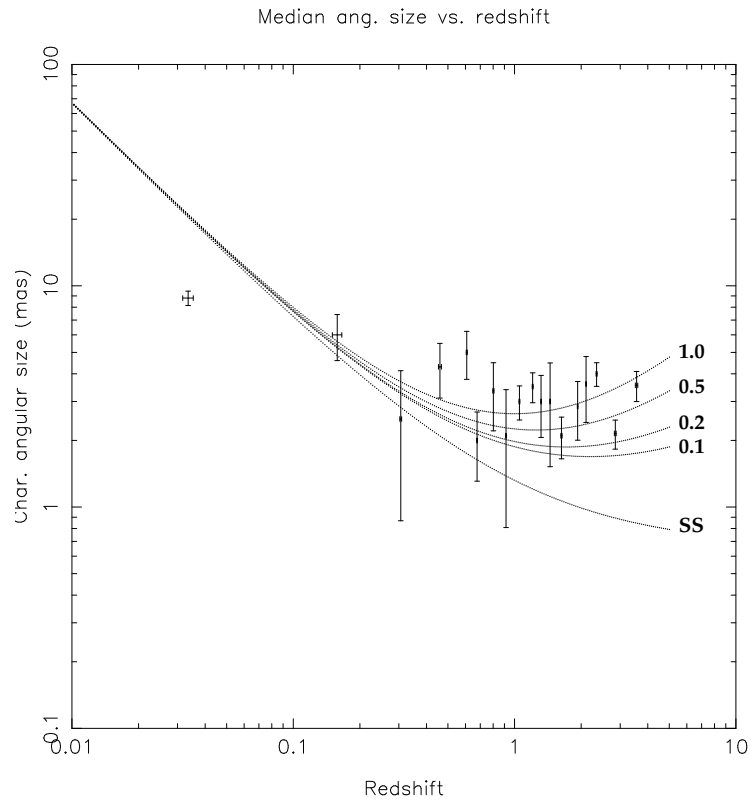


**Fig. 5.** Median angular size versus redshift. The full length of error bars here and in other figures corresponds to  $1\sigma$ . The solid lines correspond to the linear size parameter  $lh = 9.6$  pc, the Steady-state model (SS) and models of a homogeneous, isotropic Universe with  $\Lambda = 0$  and values of  $q_0 = 1.0, 0.5, 0.2, 0.1$  (as marked on the plot). Data are binned into 18 bins nearly equally populated (18–19 sources per bin).

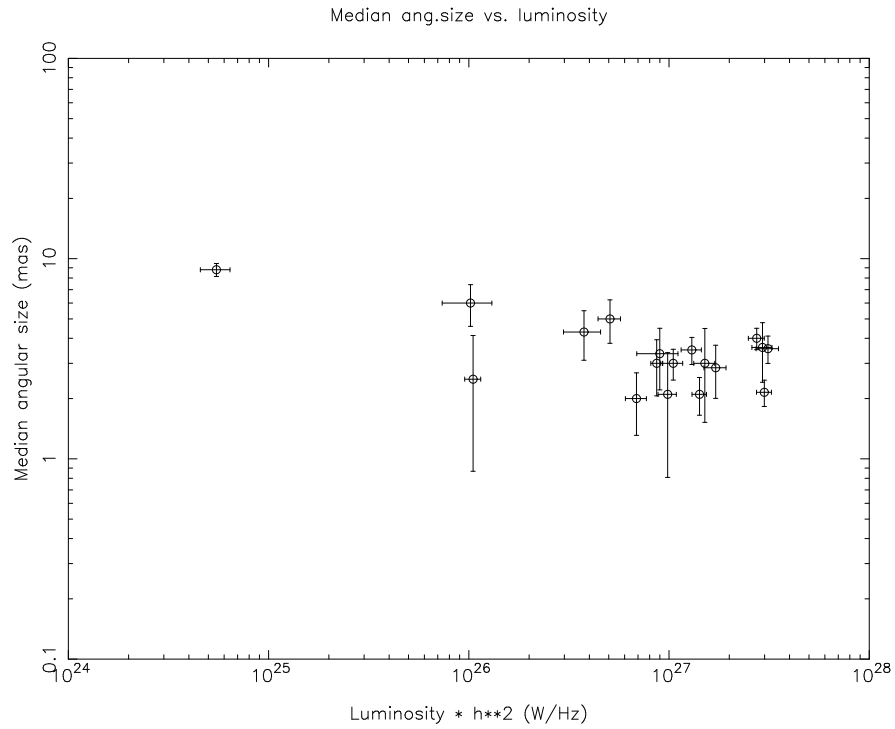


**Fig. 6.** Median angular size versus luminosity for 18 bins in redshift space (the same as in Fig. 5).

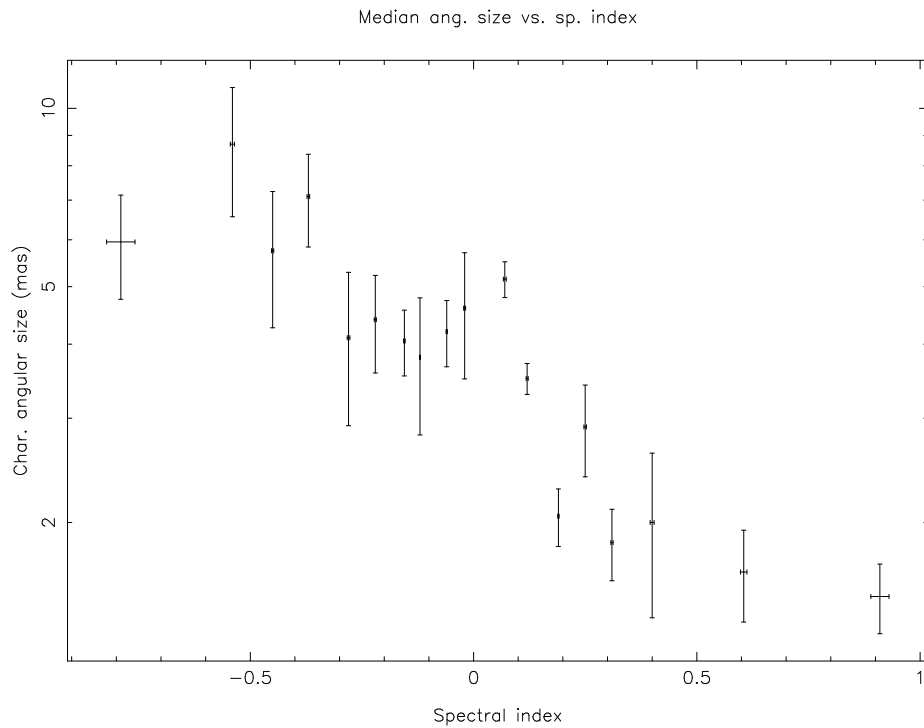


**Fig. 7.** Median angular size as a function of spectral index (the same binning in redshift space as in Fig. 5).

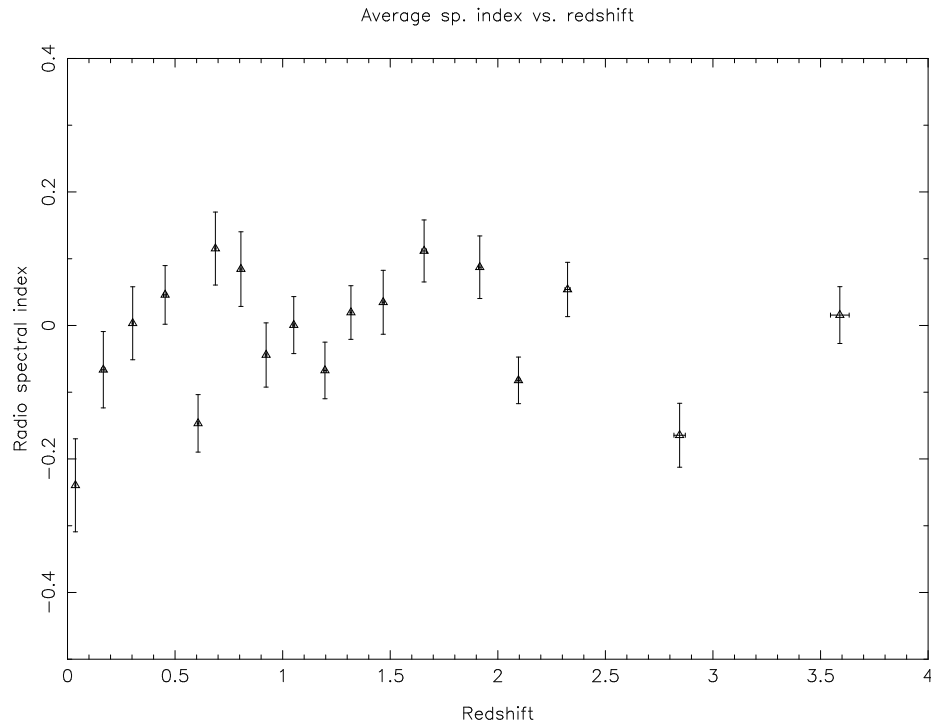


**Fig. 8.** Spectral index versus redshift (the same binning in redshift space as in Fig. 5).

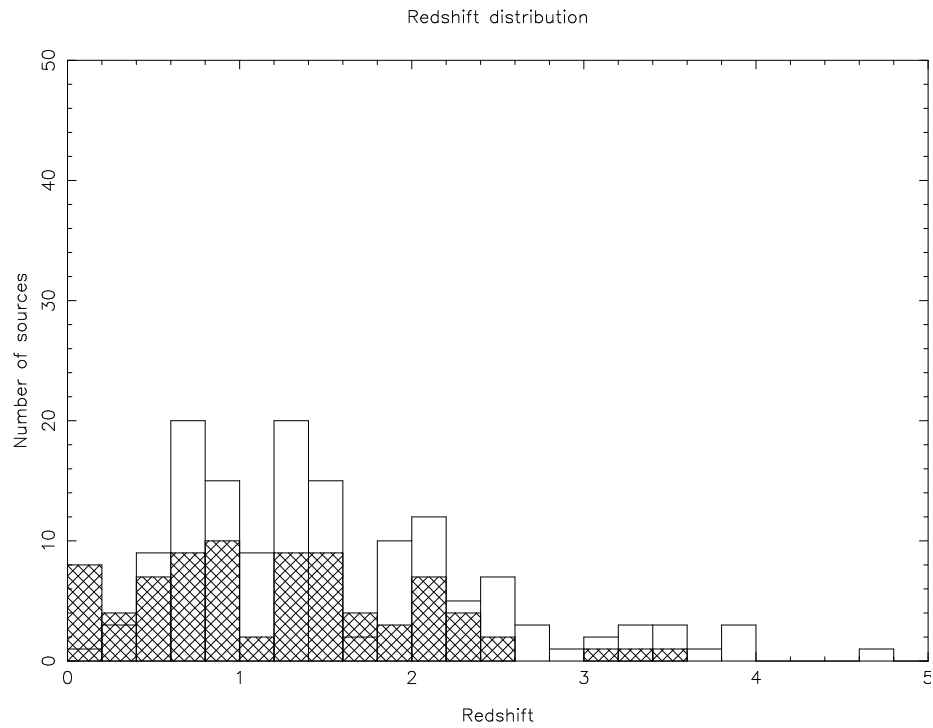


**Fig. 9.** Redshift distribution for 145 sources with  $L \geq 10^{26}$  W/Hz and  $-0.38 \leq \alpha \leq 0.18$ . Shaded part of the histogram represents the 79 sources from Kellermann (1993).

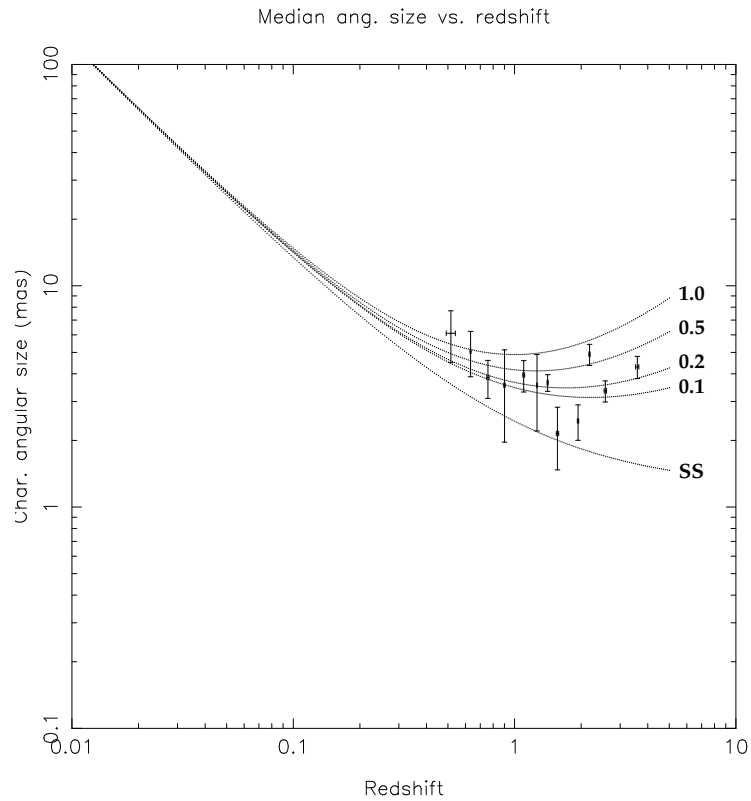


**Fig. 10.** Median angular size versus redshift for 145 sources (binned into 12 bins, 12–13 sources per bin) with  $-0.38 \leq \alpha \leq 0.18$  and  $L \geq 10^{26}$  W/Hz. The solid lines correspond to the linear size parameter  $lh = 22.7$  pc, the Steady-state model (SS) and models of a homogeneous, isotropic Universe with  $\Lambda = 0$  and various shown values of  $q_0$ . None of the solid lines represents the best fit.